IEEE Access
Multidisciplinary | Rapid Review | Open Access Journal

Received 16 July 2024, accepted 9 August 2024, date of publication 14 August 2024, date of current version 22 August 2024.

Digital Object Identifier 10.1109/ACCESS.2024.3443426

RESEARCH ARTICLE

Utilizing a Fruit Fly-Based Optimization Methodology for Reactor Placement Planning in Underground Transmission Systems

SHYH-JIER HUANG[1], (Senior Member, IEEE), CHAO-YUN TSAI[1], HSIANG-YU HSIEH[1], AND WEI-FU SU[2]

[1]Department of Electrical Engineering, National Cheng Kung University, Tainan 701, Taiwan
[2]Department of Electrical Engineering, Kun Shan University, Tainan 710, Taiwan

Corresponding author: Shyh-Jier Huang (clhuang@mail.ncku.edu.tw)

ABSTRACT This paper proposes an Enhanced Fruit Fly-Based Optimization (EFFO) approach to optimize the placement of reactors in an underground transmission system with the consideration of fluctuating loads. The EFFO method is inspired by the foraging behavior of fruit flies, which assists in the effective optimization of problem-solving. In this study, a mathematical model is developed to establish relationships among interconnected reactors, sheath loss, and induced voltage. The method integrates sheath loss with installation costs in the formulation of the objective function, providing intelligent decisions about reactor placement in underground transmission systems. Furthermore, the study addresses diverse load currents, ensuring that placement decisions comply with current regulations and are suitable for practical operations. To validate the proposed method, simulation tests are conducted on two underground transmission systems and compared with alternative methods. The simulation results demonstrate that the proposed approach effectively reduces sheath losses and exhibits satisfactory compensating performance. This study serves as a valuable reference for decision-making in the design and planning of underground transmission systems.

INDEX TERMS Underground cable, improved fruit fly optimization algorithm, sheath loss.

I. INTRODUCTION

Ensuring the quality and reliability of the power supply stands as a foremost area of concern. With the changes in economic structure and societal patterns, if the stability of power transmission lines is inadequate, it will inevitably impact the overall efficiency of the power system operation and even accelerate line aging and damage, leading to additional economic losses [1], [2], [3]. Therefore, power companies are steadfastly committed to fortifying the infrastructure of transmission lines and implementing a spectrum of protective measures aimed at bolstering the stability and resilience of the power transmission system [4].

By observing the rapid development of power technology and urbanization in recent years, the 69 kV and 161 kV underground power transmission systems have been deployed and applied in science parks, industrial areas, and metropolitan regions in Taiwan. Underground transmission not only reduces susceptibility to external environmental influences but also contributes to urban beautification. However, the extensive use of underground cables has also given rise to new operational issues. For in- stance, single-core shielded cables are susceptible to the magnetic linkage between high-voltage conductors, shielding conductors, and grounding, leading to induced voltage and circulating currents on the cable sheath [5], [6]. If the induced voltage becomes too high, it may cause electric shock incidents for construction personnel. Likewise, excessive circulating currents may result in cable overheating and increase the sheath losses of the

The associate editor coordinating the review of this manuscript and approving it for publication was Tariq Masood.

lines [7]. Regarding the use of underground cables, there are already different regulations made based on their transmission levels. The way of effectively improving the operational efficiency of these cables has become an important research topic for academic studies and power industry operation departments [8].

Currently, the main type of underground cables used in domestic installations of Taiwan is cross-linked polyethylene (XLPE) cable. To balance the three-phase induced voltage on the shielding copper wires of the cable and reduce circulating currents, it is common to employ a cross-bonding method to group three segments while the cable shielding layer is grounded at both ends [9], [10], [11]. Yet in practical operations, it is challenging to ensure a perfectly uniform and equal distance between each segment due to construction difficulties and environmental factors. Consequently, there have been studies proposing alternative strategies to reduce sheath losses. For example, a method was suggested based on the adjusting the arrangement of cable lines to decrease sheath losses [12]. Nevertheless, this method was not suitable for improving existing underground power transmission systems and did not account for additional costs that may arise from the increased terrain-related cable length. Another study proposed the use of cable sheath voltage limiters [13]. However, these voltage limiters may have different specifications depending on the cable type, and the equipment itself also requires regular inspection and maintenance. Additionally, some literature has adopted a grounding method to improve the cable operation [14]. The main concept is to ground both ends of the cable sheath without the need for an additional common grounding wire. In other words, one of the phases of the three-phase cable sheath is utilized as the common grounding wire. The demerits of this method may lie in the need of specific grounding protection devices, by which its compatibility and applicability to domestic underground power transmission systems needs careful evaluation.

Based on the literature discussed above, this study applies an improved fruit fly optimization algorithm to plan the installation of compensating reactors for underground power transmission systems [15]. The planning decision takes sheath losses and installation costs into account, considering both full load and varying load currents. The aim is to enhance the transmission quality of the power grid while also considering economic efficiency [9], [11], [16]. While numerous individuals have raised doubts regarding the proliferation of heuristic algorithms, the No Free Lunch (NFL) theorem indicates that if an algorithm excels over the other algorithm in solving a certain problem, it does not guarantee similar superiority in tackling the other problem [17]. In other words, there is no universal algorithm capable of optimizing all problems. Consequently, given the increasing complexity of problem domains, the academic community continues to encourage the development of diverse optimization algorithms. The distinctive features of this research are presented below:

1) By integrating sheath loss and installation costs into the objective function for making decisions about reactor placement, this study takes the diverse load currents into consideration, offering solutions that not only conform to current regulations but also align more closely with practical operations.
2) In contrast to existing optimization algorithms, the method introduced in this study incorporates an additional position-updating mechanism in tandem with a search enhancement technique. This enhanced approach has demonstrated its effectiveness in addressing the specific problem under consideration
3) The proposed method is systematic and can be seamlessly integrated into any commercial software for utility planning applications.

The proposed method was tested on two real underground systems in Taiwan, and the obtained results were compared with those achieved using existing methods. The remainder of this paper is organized as follows: Section II describes the paradigm of reactor placement problem, Section III presents the proposed method and its computation procedure, Section IV discusses the numerical tests, and Section V draws conclusions.

II. PROBLEM DESCRIPTIONS

A. MODELING OF UNDERGROUND CABLE SHEATH

Cross-bonding is the grounding implementation of cable routes using three consecutive manholes as a group, as shown in Figure 1. In the figure, D1, D2, D3, and D4 represent the manhole numbers, while d1, d2, and d3 represent the lengths of each section. The first manhole (D1) utilizes a regular joint box, with the metallic sheaths on both sides of the joint box continuously connected, and the three-phase sheaths are grounded together. On the other hand, the second manhole (D2) and the third manhole (D3) use insulated joint boxes to rearrange the sheaths in sequence through protective devices, effectively reducing the sheath-induced voltage. Fig. 2 illustrates the distribution of the sheath-induced voltage.

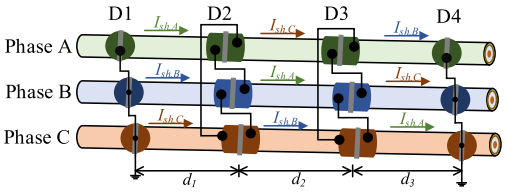

FIGURE 1. Diagram of cross-bonding.

Fig. 3 shows the equivalent circuit diagram of the cable sheath. As depicted in the figure, this paper focuses on series-connected compensating inductors at the second phase swapping location of the three-phase cable. The circulating currents in the three-phase sheaths can be obtained from (1), as shown at the bottom of the next page, where V_A, V_B, and V_C represent the sheath-induced voltages of the three-phase

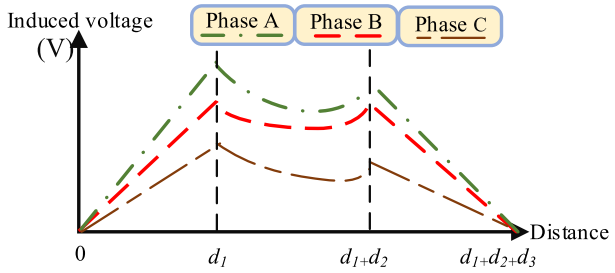

FIGURE 2. Sheath-induced voltage distribution of cross-bonding.

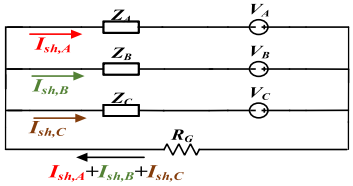

FIGURE 3. Equivalent circuit diagram of the cable sheath.

cable, and R_G is the ground resistance, whose value can be obtained from the following calculation:

$$V_n = \sum_{i=1}^{3} j\omega \times d_i \times M_{nm} \times I_L \tag{2}$$

where V_n represents the sheath-induced voltage of the nth phase of the cable, ω is the angular frequency, d_i is the distance of the ith segment, $I_L$is the load current, and M_{nm} is the coupling inductance coefficient of the nth phase cable sheath affected by the load current of the mth phase. Its calculation is done as follows:

$$\begin{cases} M_{nm} = 2 \times 10^{-4} \ln \dfrac{D_e}{x_{nm}}, & if\ m \neq n \\ M_{nm} = 2 \times 10^{-4} \ln \dfrac{D_e}{r_s}, & if\ m = n \end{cases} \tag{3}$$

where r_s is the average radius of the cable's shielding copper wire, x_{nm} is the mutual spacing between the nth phase cable and the mth phase cable, and D_e represents the skin depth when the shielding layer acts as a loop with the ground. In (1), Z_A, Z_B, and Z_C represent the sheath impedances of three phases, and their calculation are shown as follows:

$$Z_n = \sum_{i=1}^{3} Z_i + R_J + jwL_n \tag{4}$$

$$Z_i = d_i \times (R_{sh} + jX_{sh}) \tag{5}$$

where Z_n represents the sheath impedance of the nth phase cable, R_J is the connection resistance, L_n is the value of the compensating reactor added to the nth phase, Z_i represents the sheath impedance of the ith segment, R_{sh} denotes the sheath resistance, and X_{sh} represents the sheath reactance. The sheath reactance may vary depending on the cable arrangement and mutual spacing, and its calculation is performed below:

$$X_{sh} = 2\omega \times 10^{-4} \ln \frac{\sqrt[3]{x_{AB}x_{BC}x_{CA}}}{r_s} \tag{6}$$

where r_s is the average radius of the cable's shielding copper wire, and x_{AB}, x_{BC}, and x_{AC} represent the mutual spacing between the cables.

B. FORMULATION OF OBJECTIVE FUNCTIONS

When addressing the planning of compensation inductance installation, this article simultaneously encompasses the goals of minimizing both sheath loss and installation cost within the framework of its objective function. First, concerning the sheath loss of P_{sl} after adding compensation reactor to the system, it is calculated as follows:

$$P_{sl} = \sum_{i=1}^{j} \sum_{n=1}^{p} R_{sh} \cdot d_i \cdot \left| I_{sh,n} \right|^2 \tag{7}$$

where j and p represent the total number of segments and total phases of the underground cable system, respectively. To achieve the solution consistency, it is necessary to normalize the sheath loss. Therefore, the first objective function f_1 is formulated as follows:

$$f_1 = \frac{P_{sl} - P_{sl}^{\min}}{P_{sl}^{\max} - P_{sl}^{\min}} \tag{8}$$

where P_{sl}^{min} is the sheath loss of the cable system after compensating with maximum capacity of reactors at all installable locations, P_{sl}^{max} is the total sheath loss before compensation, and P_{sl} is the sheath loss of the cable system prior to compensation. Furthermore, by taking economic benefits into account after installing reactors, the computation of investment is given below:

$$Cost = \sum_{n=1}^{p} C_{price,n}(L_n) \tag{9}$$

where $Cost$ represents the reactor installation cost, $C_{price,n}$ denotes the cost of compensating reactor at the nth phase, and L_n is the value of reactor for the nth phase. Through the

$$\begin{cases} I_{sh,A} = \dfrac{R_G(V_A \cdot Z_B + V_A \cdot Z_C - V_B \cdot Z_C - V_C \cdot Z_B) + V_A \cdot Z_B \cdot Z_C}{R_G(Z_A \cdot Z_B + Z_A \cdot Z_C + Z_B \cdot Z_C) + Z_A \cdot Z_B \cdot Z_C} \\ I_{sh,B} = \dfrac{R_G(V_B \cdot Z_A - V_A \cdot Z_C - V_C \cdot Z_A + V_B \cdot Z_C) + V_B \cdot Z_A \cdot Z_C}{R_G(Z_A \cdot Z_B + Z_A \cdot Z_C + Z_B \cdot Z_C) + Z_A \cdot Z_B \cdot Z_C} \\ I_{sh,C} = \dfrac{R_G(V_C \cdot Z_A - V_B \cdot Z_A - V_A \cdot Z_B + V_C \cdot Z_B) + V_C \cdot Z_A \cdot Z_B}{R_G(Z_A \cdot Z_B + Z_A \cdot Z_C + Z_B \cdot Z_C) + Z_A \cdot Z_B \cdot Z_C} \end{cases} \tag{1}$$

following normalization, the second objective function of f_2 for this study is formulated below:

$$f_2 = \frac{Cost - Cost_{min}}{Cost_{max} - Cost_{min}} \tag{10}$$

where $Cost_{min}$ and $Cost_{max}$ represent the minimum and maximum values of the reactor installation cost, respectively. Finally, based on the derived objective functions for sheath loss and installation cost, by incorporating their respective weight values, a multi-objective function model can be constructed and expressed as follows:

$$Minimizef = w_1 \times f_1 + w_2 \times f_2 \tag{11}$$

where f_1 and f_2 individually represents the objective functions for sheath loss and installation cost, and w_1 and w_2 are the weight values assigned to each function with a total weight summation of 1. Depending on practical power application requirements, the weight values can be adjusted to allocate proportions to the objective functions. Moreover, by considering the impact of induced voltage rise after reactor compensation, this study simultaneously introduces the induced voltage constraint. Given that the upper limit of the induced voltage is 65 V, the constraint is formulated as shown below:

$$V_n^{\max} \leq 65V \tag{12}$$

where V_r^{max} represents the maximum induced voltage of the nth phase cable after compensation.

III. COMPUTATION OF PROPOSED ALGORITHM

Based on the formulation of objective functions and corresponding constraints, this paper utilizes the enhanced fruit fly-based optimization (EFFO) approach for the reactor placement of underground transmission system. The aim is to utilize the excellent solving capability of this algorithm to ensure that the planning meets the optimal compensating reactor configuration requirements. This section describes the establishment of the algorithm model and the calculation process.

A. IMPROVED FRUIT FLY-BASED OPTIMIZATION ALGORITHM

The fruit fly optimization algorithm mimics the foraging behavior of fruit flies in the natural environment [18], [19], [20], [21]. The fruit fly is an insect distributed in tropical and subtropical climates, often found in areas abundant in fruits or food sources. When a fruit fly seeks food, it utilizes its snap-tentacles to detect specific odor molecules in the air. By comparing the strength of odor signals received by its two tentacles, the fruit fly determines the direction of the food source. If one tentacle receives a stronger odor signal than the other, then the fruit fly will move towards the direction of the stronger signal to locate the food. Fruit flies also communicate using chemical signals such as pheromones. If they discover the location of food, they release chemical substances to attract other fruit flies. However, during the process of foraging, fruit flies may encounter environmental changes or predator attacks. Upon detecting danger, they immediately move in a different direction to escape and avoid the threat.

Based on the aforementioned foraging behaviors of fruit flies, the equivalent relationship between the algorithm and compensation planning is first delineated. During the algorithm-solving process, the coordinates of each food source is regarded as feasible solutions for the installation planning of a set of compensation devices. The intensity of food odor represents the quality of the installation of that set of compensation devices. It is known that once the fruit fly receives signals emitted by companions located at the positions with the most significant odor of food, they would move towards that location to conduct a search. Therefore, the algorithm initially denote the fruit fly population as $\boldsymbol{F}= (F_1,F_2,\ldots F_i,\ldots F_M)$ consisting of M individual fruit flies. The position of each fruit fly represents a coordinate, equivalent to M sets of different reactor installation plans. Subsequently, the fruit fly population searches towards the direction of the food and updates their position coordinates, which is modeled by the following equation:

$$F_i(k+1) = F_i(k) + v_i(k) \tag{13}$$

$$\begin{cases} v_i(k+1) = v_i(k) + \varepsilon_i(F_{best}(k) - F_i(k)) \\ \varepsilon_i = \varepsilon_{\min} + r\,(\varepsilon_{\max} - \varepsilon_{\min}) \end{cases} \tag{14}$$

where $F_i(k)$ and $F_i(k+1)$ represent the position coordinates of the i-th fruit fly in the k-th and $k+1$-th iteration, $F_{best}(k)$ is the position coordinates of the food in the k-th iteration, $v_i(k)$ and $v_i(k+1)$ represent the displacement of the i-th fruit fly in the k-th and $k+1$-th iteration, with r is a random variable ranging between 0 and 1. Meanwhile, due to variations in the sensitivity of each individual fruit fly to odor reception and differences in flying capabilities, their abilities to search for food also vary. This diversity in searching ability contributes to differences in effectiveness. Therefore, in (14) of this mechanism, distinct flying abilities are assigned to each fruit fly to enhance the diversity of their movement speeds. This, in turn, increases the likelihood of finding high-quality solutions, where ε_i represents the searching ability of the i-th fruit fly, while $\varepsilon_{\max}$ and $\varepsilon_{\min}$ denote the upper and lower limits of searching ability.

After establishing the fruit fly food search mechanism, this paper proceeds to introduce the adverse environment mechanism. This mechanism considers the possibility that fruit flies might encounter weather changes or predator attacks while searching for food in their natural environment. In other words, when unfavorable survival factors are detected during the food search process, fruit flies will promptly alter their flight direction to avoid harm. The mathematical model for this mechanism is presented

as follows:

$$F_i(k+1) = F_i(k) + H \times (F_{\max} - F_{\min}), \textit{if} \;\; p < \mu \quad (15)$$

$$H(x) = \frac{\Gamma\left(\frac{v+1}{2}\right)}{\Gamma\left(\frac{v}{2}\right)} \frac{1}{\sqrt{v\pi}} \frac{1}{(1+\frac{x^2}{v})^{\frac{v+1}{2}}} \quad (16)$$

where F_{min} and F_{max} are the lower and upper limits of the control variable, $H(x)$ represents the probability density function of the t-distribution (Student's t-distribution), Γ is the Gamma distribution function, v stands for the degrees of freedom of the t-distribution, and x is a random variable following the t-distribution. Through this probability density function, the diversity of feasible solutions can be increased, hence benefiting the global search capability.

Building upon the previously discussed algorithm, we present an enhanced fruit fly optimization algorithm (EFFO). The motivation behind this enhancement lies in the behavior of the original method, where the fruit fly with the highest food odor value does not respond to the pheromones released by other fruit flies, potentially resulting in limited movement. Such practice may overlook detailed searching and could potentially get trapped in local solutions. Hence, this paper strategically integrates a search enhancement technique to amplify exploration in the proximity of the current optimal solution, fortifying the search within its immediate vicinity. This increases solution variability, providing an opportunity to escape local solutions and find a globally better solution. The mathematical modeling of this search enhancement is presented below:

$$F_i(k+1) = F_{best}(k) + \tau R(k) \textit{if} \;\; rand > s_i(k) \quad (17)$$

$$\begin{cases} R_i(k+1) = \alpha R_i(k) \\ s_i(k+1) = \beta\left[1 - \exp(-k)\right] \end{cases} \quad (18)$$

The above equation first determines whether to initiate detailed searching through a probability function. In other words, if the random value (*rand*) is greater than the probability $s_i(k)$ of the i-th fruit fly executing the search enhancement method at the kth iteration, then the detailed movement is performed. Here, τ is a random number ranging from -1 to 1, $R_i(k)$ and $R_i(k+1)$ represent the search enhancement ranges of the i-th fruit fly at the k-th and $(k+1)$-th iterations, *rand* is a random variable between 0 and 1, α is the range parameter, and β is the probability of triggering of the search enhancement. After executing the search enhancement, the objective function value at the new location is calculated when moving to the new location. This value is then compared to the objective function value of the existing best solution, $F_{best}(k)$. If the objective value at the new location is lower than that of the current best solution, the new location would supersede the original best solution, resulting in the emergence of a new optimal solution. This is equivalent to finding a better plan of reactor placement.

B. COMPUTATION PROCEDURE

Fig. 4 is a schematic diagram of the improved fruit fly optimization algorithm process. As depicted in the figure, this approach initiates by gathering data from the underground cable system, which is essential for simulating the planning of compensation device installations. Meanwhile, cable specifications, cable arrangements, cable lengths for each segment, and cable load current data are all input into the algorithm. Subsequently, constraints related to the safe operation regulations for underground cables are established, followed by the configuration of algorithm-related parameters.

Once the system data and algorithm-related parameters have been configured, a population of fruit flies comprising M positions is generated. The fruit fly population can be represented as $\boldsymbol{F} = [F_1, F_2, \ldots, F_i, \ldots, F_M]$, and the control variables for solving the optimization problem are equivalent to the positions of the fruit flies, represented as $F_{\mathbf{i}} = [f_{i,1}, f_{i,2}, \ldots, f_{i,j}, \ldots, f_{i,N}]$, where $f_{i,j}$ represents the j-th position of the i-th fruit fly. Within the framework of the issue addressed in this paper, aimed at enhancing cable insulation loss, each $f_{i,j}$ can be regarded as the reactance necessary for compensating the j-th phase of the sheath. There exist N phases of sheaths where compensatory devices can be deployed. A value of 0 indicates that no compensation inductance is required for that particular sheath phase.

Next, the food odor values corresponding to the positions of each fruit fly are computed, reflecting the objective function values for each feasible solution group. After inputting the coordinates of each fruit fly's position into the objective function, the respective objective function values for each fruit fly's position can be determined. Subsequently, these objective function values are sorted. It is also noted here that this paper frames reactor placement planning as a minimization problem, where lower objective function values signify greater improvements in power transmission quality and cost-effective installation.

After assessing the quality of each fruit fly's position, the fruit fly searching for food mechanism is executed, followed by the adverse environment mechanism, which is the search enhancement method to update the positions of the fruit flies. Next, the food odor values at the new positions are compared with those at the previous positions. If the odor value is higher after the movement, the fruit fly's position is updated, replacing the original position. Conversely, if the odor value at the new position is not higher than the previous one, the fruit fly remains in its original position.

The fruit fly population undergoes continuous updates via the previously mentioned mechanism. With each increased iteration, the fruit flies progressively converge towards the location with the highest odor value, signifying the ongoing refinement of feasible solutions toward the optimal solution. The output decoding result of this best solution signifies the precise placement location of the compensation device. This planning outcome can serve as a valuable reference for the design and planning of underground power transmission systems.

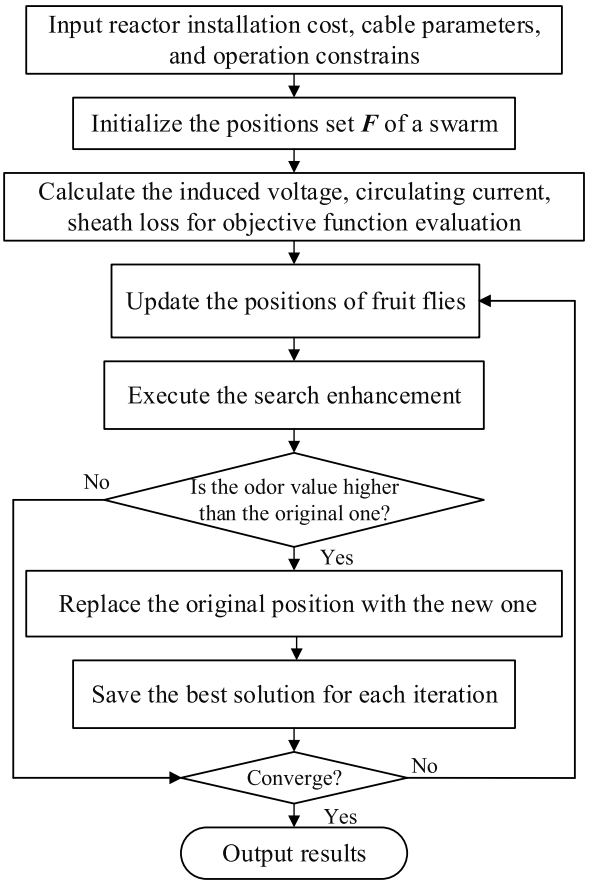

FIGURE 4. Flowchart of computation process.

IV. NUMERICAL STUDIES

This paper utilizes the improved fruit fly optimization algorithm for the planning of underground cable compensation device installation, with the aim of maximizing the effectiveness of the device placement. The algorithm is configured with a maximum iteration limit of 150 iterations, a population of 100 fruit flies, and search enhancement range and triggering probability parameters set to 0.9. Once the iteration count, fruit fly population size, and power transmission system parameters are all determined, the calculation process begins.

A. TEST 1

Fig. 5 shows the system architecture of test 1, where the circuit is divided into six segments from substation E/S to C/S. Each manhole in this system is individually labeled as D1 to D5, with D1 being the closest to substation E/S and D5 being the farthest away. This test line is divided into two alternating grounding segments: E/S to D3 and D3 to C/S, with a total length of approximately 1.9 kilometers. Both underground cables in the test lines of this system use 161 kV cross-linked polyethylene cables, as specified in Table 1. As shown in the table, this system operates in a dual-circuit configuration with a conductor size of 2000 mm^2 for each single-core copper conductor, which is capable of transmitting a rated current

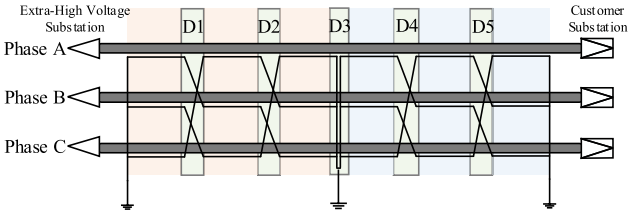

FIGURE 5. System architecture of test 1.

TABLE 1. Cable specification of test 1.

Section	Segment Distance (km)	Mutual Distance between cables (mm)	Three-phase cable placement
E/S to D1	0.375	115	
D1 to D2	0.371	115	
D2 to D3	0.357	115	
D3 to D4	0.2304	115	
D4 to D5	0.317	115	
D5 to C/S	0.235	115	

of 1080 A. The primary focus of this test line is on phase A, B, and C, while X, Y, and Z form another parallel circuit. Therefore, when investigating the primary circuit, it is also necessary to consider the effects generated by the parallel circuit.

1) SCENARIO 1: FULL LOAD CURRENT

This simulation scenario aims to investigate the operational conditions and compensation of cable sheaths when both circuits are at full load current. The simulation includes the induced voltage limit to ensure the reactor compensation planning meets the requirement of safe voltage operation. Table 2 presents the compensation results for this scenario. From the table, it can be observed that the total three-phase sheath losses have decreased from 1714.3 W to 147.97 W after the compensation. There is a decreasing trend in the three-phase sheath circulating current after the compensation. Fig. 6 illustrates the distribution of induced voltage with and without the compensation. It is evident that the arrangement of test line is relatively symmetrical, but there is a difference

TABLE 2. Compensation results of scenario 1.

	E/S to D3	D3 to C/S
Compensation reactor (mH)	0.2, Phase A 0.15, Phase B 0.05, Phase C	0.7, Phase A 0.7, Phase B 0.6, Phase C
Installation cost	5.26 p.u.	
Sheath loss before the compensation	1714.3 W	
Sheath oss after the compensation	147.97 W	

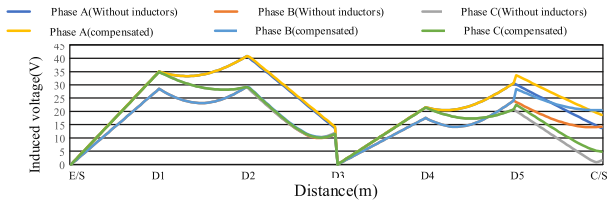

FIGURE 6. Distribution of induced voltage with and without the compensation.

in segment lengths, particularly in the D3 to C/S section due to topographical factors. Consequently, this section exhibits a higher maximum induced voltage and sheath circulating current compared to the E/S to D3 section, exhibiting the improvement in the sheath operation. The compensation strategy proposed in this paper hence suggests installing a larger reactor in this section, leading to a relatively greater increase in three-phase induced voltage. It is, however, worth noting that at any point in each segment, this induced voltage remains within the safety standard of 65V.

2) SCENARIO 2: VARYING LOAD CURRENT

To align reactor deployment more closely with actual conditions, this simulation scenario involves applying various daily load currents to the sheath operation model of the test line. Since this system belongs to a dual-circuit coaxial cable system, the load currents of the line will mutually induce each other's cable sheath layers. Therefore, when seeking the reactor compensation, it is necessary to simultaneously consider the coexistence mode and operational status of both lines. Taking the calculation of phases A, B, and C as an example, when formulating the sheath operation model for the whole day, it is necessary to consider the load current of the main circuit during that time period and pay attention to load currents of adjacent coexisting lines, namely phases X, Y, and Z. Fig. 7 shows the daily load current curves of phase ABC and XYZ of the test lines. As depicted in the figures, the maximum load current for phase ABC occurs at 8 AM with a peak value of 1080 A. On the other hand, the maximum load current for the coexisting line XYZ occurs at 10 PM with a peak value of 1017.36 A.

Next, the daily load current curves of the aforementioned test lines, the cable lengths in various sections, the way of

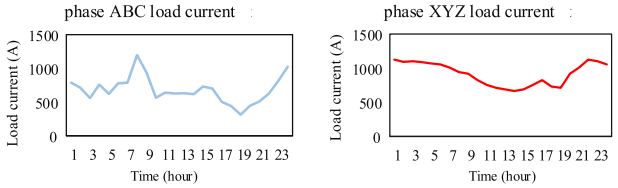

FIGURE 7. Load current of test line on the whole day.

arrangement, and cable spacings are delivered to the cable sheath calculation model to obtain simulation results for computing daily sheath losses. This testing system comprises two sets of interleaved grounding, requiring the installation of six compensation reactors connected in series to the cable sheath of phases A, B, and C in the grounding sections. Through the calculation, the capacity for each compensation reactor can be determined. Table 3 shows the compensation results of this scenario 2. For the E/S to D3 section, the tabulation shows that there is no need to install compensation reactors. The main difference between scenario 1 and 2 lies in that for scenario 1, the load current increases when operating at full load, leading to a larger per-phase circulating current, and therefore, the installation of compensation reactors per phase can significantly suppress core losses. However, for scenario 2 with varying load currents, the line is not operated at full load for extended periods, resulting in smaller per-phase circulating currents over time. There is less room for improvement in core losses. Hence, after evaluating the reduction in sheath losses and the desired increase in installation costs for this section, the algorithm suggests that compensation devices may not be needed.

TABLE 3. Compensation results of scenario 2.

	E/S to D3	D3 to C/S
Compensation reactor (mH)	0, Phase A 0, Phase B 0, Phase C	0.75, Phase A 0.75, Phase B 0.75, Phase C
Installation cost	3.89 p.u.	
Sheath loss before the compensation	14497.58 W	
Sheath loss after the compensation	1253.89 W	

Fig. 8 plots the sheath current of phase A before and after compensation in the section of D3 to C/S. As shown in the figure, after installing compensation reactors, both the daily three-phase circulating currents and the daily maximum circulating currents in this section are significantly decreased. Moreover, the maximum induced voltages at each phase after connecting the compensation reactors do not exceed the rated operating standards. The sheath losses of a whole day have also decreased from 14,497.58 W to 1,269.4 W. These test results demonstrate that the method proposed in this paper offers better economic benefits.

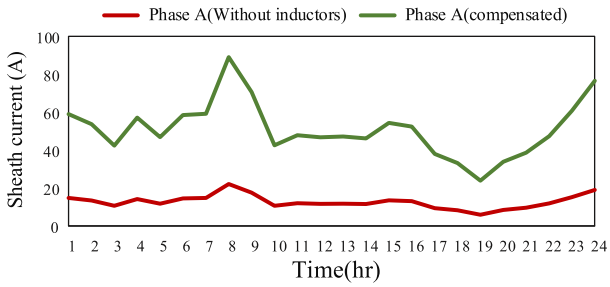

FIGURE 8. Sheath current of phase A before and after compensation in the section of D3 to C/S.

To further verify the performance of the method, this test case compares the simulation results of each method presented in Table 4 and Fig. 9. Method-1 is the particle swarm optimization algorithm, Method-2 is the fruit fly optimization algorithm, and Method-3 is the improved fruit fly optimization algorithm. For each method, Table 4 lists the minimum, average, and maximum objective function values, average computation time, and standard deviation after 50 trials. A smaller standard deviation indicates that most of the optimal solutions are close to the average value. Although the minimum objective function values for various methods are similar, Method-3 yields relatively smaller maximum values, average values, and standard deviations. This suggests that the proposed method has better convergence properties compared to the other methods. However, its average computation time is slightly longer than that of the other two methods. Fig. 9 depicts the frequency distribution of objective functions for each method. The figure clearly shows that Method-3 exhibits a notably higher frequency of superior objective function solutions, demonstrating the stability and outstanding performance of the method introduced in this paper.

TABLE 4. Convergence results for test 1.

Approach	Method-1	Method-2	Method-3
Maximum	0.2233	0.2217	0.2141
Minimum	0.2125	0.2125	0.2125
Average	0.2194	0.2176	0.2128
Standard deviation	0.0037	0.0022	0.0007
Average computation time	5.54	5.34	5.75

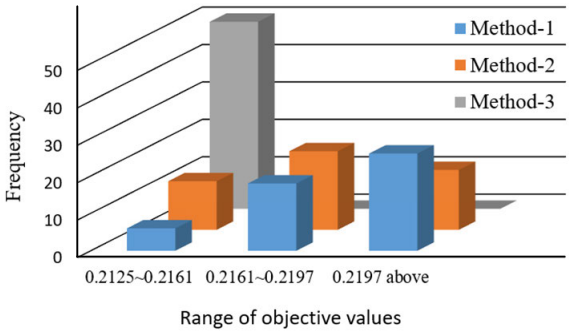

FIGURE 9. Frequency of convergence for test 1.

B. TEST 2

The circuit in this test 2 is a co-constructed underground cable system in Taiwan, where all four lines use 2,000 mm^2 cross-linked polyethylene cables with a transmission voltage level of 161 kV and a rated operating current of 1,194 A. Fig. 10 is the system architecture of test line. As shown in the figure, the line is divided into nine sections from the ultra-high-voltage substation E/S to the distribution substation D/S. The cables are grounded using three sets of cross-connections. In this system, each of these manholes in the system is named F1 to F7, with F1 being the closest to the ultra-high-voltage substation E/S and F7 being the farthest. Due to different co-construction line configurations and arrangements in various sections of this test line, and the mutual induction of load currents on each other's cable sheaths, this paper takes the segment length, the number of lines, and the arrangement into considerations when determining the compensation device strategy as shown in Table 5. From the table, it is seen that the system from E/S to F1 is a single-circuit system, which is the main focus of this section consisting of phases A, B, and C, individually. The F1 to F4 sections are co-constructed with another double-circuit underground cable line, making it a four-circuit system, while the remaining sections are double-circuit co-construction systems. This line is divided into nine segments with cable grounds via the way of cross-connection. The total length of the line spans approximately 2.2 kilometers, segmented into three groups of cross-connected grounding segments: from E/S to F3, from F3 to F6, and from F6 to D/S.

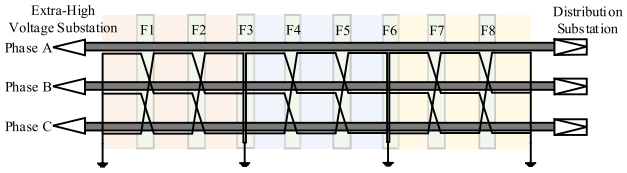

FIGURE 10. System architecture of test 2.

1) SCENARIO 1: FULL LOAD CURRENT

In this simulation scenario, the three-phase load currents of all four co-constructed circuits are modeled at their full load capacity of 1,194 A. The simulation is carried out separately for the sections from E/S to F3, F3 to F6, and F6 to D/S to analyze their operating conditions before the placement of reactors. The arrangement of each section, the segment length, and the load currents for each phase of the cables are all input into the calculation model to determine the induced voltage and circulating current for each section, by which the sheath losses before the reactor compensation are computed.

Following the completion of aforementioned calculations, the study proceeds to determine the compensation strategy

via the proposed algorithm. The test circuit encompasses a larger-scale underground cable system spanning approximately 2.2 kilometers in total length, encompassing three sets of cross-connected grounding. Consequently, the installation necessitates nine compensation reactors. These reactors are strategically connected to the sheaths of A, B, and C phase cables within these three cross-connected grounding regions, specifically spanning from E/S to F3, from F3 to F6, and from F6 to D/S.

TABLE 5. Cable specification of test 2.

Section	Segment Distance (km)	Mutual Distance between cables (mm)	Three-phase cable placement
E/S to F1	0.2569	A-B 115 B-C 115 C-A 115	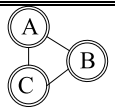
F1 to F2	0.2502	A-B 220 B-C 220 C-A 310	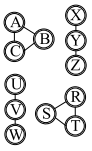
F2 to F3	0.2026	A-B 220 B-C 220 C-A 310	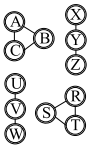
F3 to F4	0.2465	A-B 490 B-C 220 C-A 310	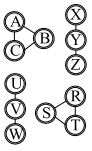
F4 to F5	0.2554	A-B 310 B-C 310 C-A 620	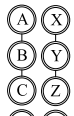
F5 to F6	0.2576	A-B 310 B-C 310 C-A 620	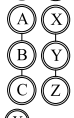
F6 to F7	0.2531	A-B 310 B-C 310 C-A 438	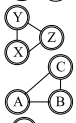
F7 to F8	0.2418	A-B 310 B-C 310 C-A 620	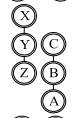
F8 to D/S	0.2323	A-B 310 B-C 310 C-A 620	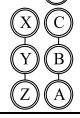

Table 6 tabulates the compensation results of this scenario. The installation cost for this case is 6.64 p.u. Due to the different arrangement in the section from E/S to F3 and the spacing between phases, it requires the installation of larger-capacity compensation reactors. The total sheath losses for all three phases can be reduced from 5859.45 W to 557.49 W. Fig. 11 shows the distribution of induced voltages before and after compensation under this scenario one. The figure reveals that both before and after installing the compensation reactors, the maximum induced voltage does not exceed the specified limit of 65 V, aligning with the cable's operational requirements.

TABLE 6. Compensation results of scenario 1.

	E/S to F3	F3 to F6	F6 to D/S
Compensation reactor (mH)	0.8, Phase A 0.4, Phase B 0.2, Phase C	0.5, Phase A 0.15, Phase B 0.2, Phase C	0.1, Phase A 0, Phase B 0.05, Phase C
Installation cost	6.64 p.u.		
Sheath Loss before the compensation	5859.45 W		
Sheath Loss after the compensation	557.49 W		

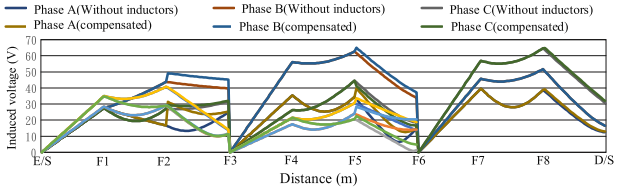

FIGURE 11. Distribution of induced voltage with and without the compensation.

2) SCENARIO 2: VARYING LOAD CURRENT

This scenario explores the compensation planning under varying load currents. Fig. 12 displays the daily load current curves for this tested system, where the maximum load current for phases A, B, and C occurs at 10 PM, while the minimum load occurs at 6 AM. For phases U, V, and W, the maximum load current happens at 12 AM, and the minimum load occurs at 8 AM. Phases R, S, and T experience their maximum load current at 4 PM, with the minimum load occurring at 5 AM. Finally, phases X, Y, and Z reach their maximum load current at 10 PM with the minimum load occurring at 2 PM.

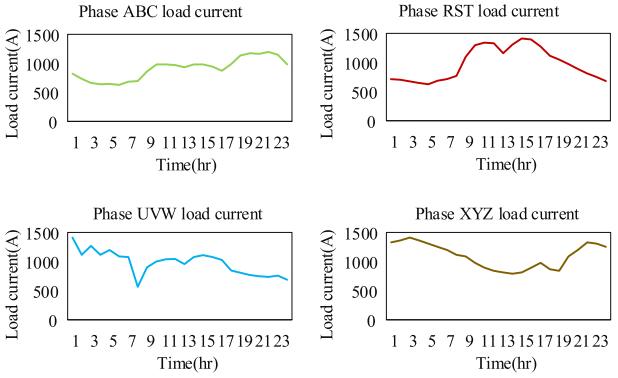

FIGURE 12. Load current of test line on the whole day.

This transmission line consists of three intersecting junctions, where nine compensation reactors can be added, each installed on the sheath of the A, B, and C three-phase cables from E/S to F3, F3 to F6, and F6 to D/S, as shown in Table 7 for the simulation results. From the table, it can be observed that within the section from F6 to D/S, the circulating current is lower due to the similar arrangement and permutation length. Under non-full load conditions, the sheath loss is very limited. Therefore, the addition of compensation reactors in this section can only marginally reduce the insulation loss, yet it may significantly increase the construction cost. More attentions are suggested to pay to this outcome during the planning process. Fig. 13 plots the sheath current of phase A before and after compensation in the section of E/S to F3. As shown in the figure, the circulating current of a whole day significantly decreases after the compensation.

Table 8 presents the convergence results of each method on test 2 after conducting 50 independent experiments. Although all methods achieved similar minimum objective function values, Method-3 exhibits the smallest standard deviation. Fig. 14 shows the frequency distribution of objective function values within a specified range. The figure indicates that Method-3 has a higher probability of reaching high-quality solutions. Regardless of the testing system used for simulation, Method-3 consistently reaches the minimum value as observed from the figure and the tabulation. Furthermore, when compared to several previously published methods in multiple test results, the proposed approach demonstrates a greater ease of convergence to higher quality along with more robust solutions. This makes it suitable for application in the planning of underground cable compensation reactance, presenting a better robustness.

TABLE 7. Compensation results of scenario 2.

	E/S to F3	F3 to F6	F6 to D/S
Compensation reactor (mH)	0.8, Phase A 0.35, Phase B 0.2 Phase C	0.35, Phase A 0.5, Phase B 0, Phase C	0, Phase A 0, Phase B 0.1, Phase C
Installation cost	5.41 p.u.		
Sheath loss before the compensation	64278.14 W		
Sheath loss after the compensation	5512.90 W		

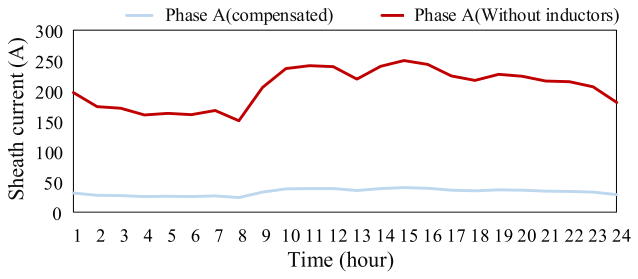

FIGURE 13. Sheath current of phase A before and after compensation in the section of E/S to F3.

TABLE 8. Convergence results of each method.

Approach	Method-1	Method-2	Method-3
Maximum	0.2169	0.2142	0.2096
Minimum	0.2093	0.2093	0.2093
Average	0.2115	0.2097	0.2094
Standard deviation	0.0023	0.0011	0.0001
Average computation time	11.46	10.68	14.15

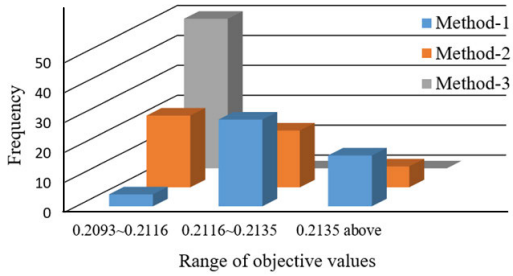

FIGURE 14. Frequency of convergence for test 2.

V. CONCLUSION

This paper proposes the application of improved fruit fly optimization algorithm in the planning of compensation inductance for underground cable systems considering both full load and variable load current scenarios. The paper establishes an objective function that includes sheath losses and the cost of installing compensation reactors. By simulating the food-seeking behavior of fruit flies, the paper also derives the mathematical model of the fruit fly optimization algorithm and supplements it with a search enhancement method to improve global search capabilities. Simulations are conducted through two practical transmission systems for the validation. The results of reactor placement planning presented in this article contribute to reducing sheath losses while taking the investment cost into considerations. This proposed approach also surpasses other methods by preventing premature convergence, rendering it highly effective for applications in reactor allocation of underground transmission systems. This study currently focuses on the planning stage. In the future research, the proximity effect, ambient electromagnetic fields, return currents, and environmental influences on cable current will be considered to achieve a model that more accurately reflects practical systems.

ACKNOWLEDGMENT

The authors are greatly indebted to Taiwan Power Company for providing their technical support and valuable operating experiences.

REFERENCES

[1] B. Patel and P. Bera, "A new transmission line parameter estimation technique and its impact on fault localization," *IEEE Trans. Instrum. Meas.*, vol. 72, pp. 1–8, 2023.

[2] G. Li, J. Chen, H. Li, L. Hu, W. Zhou, and C. Zhou, "Detection of irregular sheath current distribution for diagnosis of faults in grounding systems of cross-bonded cables," *IEEE Access*, vol. 11, pp. 68453–68461, 2023.
[3] M. A. Shokry, A. Khamlichi, F. Garnacho, J. M. Malo, and F. Álvarez, "Detection and localization of defects in cable sheath of cross-bonding configuration by sheath currents," *IEEE Trans. Power Del.*, vol. 34, no. 4, pp. 1401–1411, Aug. 2019.
[4] X. Wang, J. Yong, and L. Li, "Investigation on the implementation of the single-sheath bonding method for power cables," *IEEE Trans. Power Del.*, vol. 37, no. 2, pp. 1171–1179, Apr. 2022.
[5] R. Candela, A. Gattuso, M. Mitolo, E. R. Sanseverino, and G. Zizzo, "A model for assessing the magnitude and distribution of sheath currents in medium and high-voltage cable lines," *IEEE Trans. Ind. Appl.*, vol. 56, no. 6, pp. 6250–6257, Nov. 2020.
[6] S. Caniggia and F. Maradei, "Investigation on grounding solutions for shielded cables by simple SPICE models," *IEEE Electromagn. Compat. Mag.*, vol. 11, no. 2, pp. 61–69, Aug. 2022.
[7] *IEEE Standard for Harmonic Control in Electric Power Systems*, IEEE Standard 519-2022, 2022.
[8] *IEEE Guide for Bonding Shields and Sheaths of Single-Conductor Power Cables Rated 5 KV Through 500 KV*, IEEE Standard 575-2014, 2014.
[9] A. Das and C. C. Reddy, "Sheath voltage and sheath current phenomenon for different types of bonding for HV power cable under steady state," in *Proc. IEEE 6th Int. Conf. Condition Assessment Techn. Electr. Syst. (CATCON)*, Dec. 2022, pp. 202–206.
[10] R. Arunjothi and K. P. Meena, "Sheath overvoltage on 220 kV XLPE cable under fault conditions," in *Proc. 22nd Int. Symp. High Voltage Eng. (ISH)*, Nov. 2021, pp. 320–325.
[11] S. M. Noufal and G. J. Anders, "Sheath loss factor for cross-bonded cable systems with unknown minor section lengths—Field verification of the IEC standard," *IEEE Trans. Power Del.*, vol. 35, no. 6, pp. 2722–2730, Dec. 2020.
[12] Z. Li, Y. Chu, Q. Li, X. Liu, H. Xu, X. Guo, and J. Li, "Study on sheath grounding mode and reasonable arrangement of return line for parallel cables," in *Proc. 16th IET Int. Conf. AC DC Power Transmiss. (ACDC)*, vol. 2020, Jul. 2020, pp. 2248–2252.
[13] P. Maneepeth, P. Tharatak, P. Jirapong, and C. Karaaom, "Mitigation of induced currents and overvoltages in metallic sheath of 115 kV underground cable using sheath voltage limiter and parallel ground continuity conductor," in *Proc. 9th Int. Electr. Eng. Congr. (iEECON)*, Mar. 2021, pp. 61–64.
[14] L. Li, J. Yong, and W. Xu, "Single-sheath bonding—A new method to bond/ground cable sheaths," *IEEE Trans. Power Del.*, vol. 35, no. 2, pp. 1065–1068, Apr. 2020.
[15] S. J. Huang, X. Z. Liu, W. F. Su, and S. H. Yang, "Application of hybrid firefly algorithm for sheath loss reduction of underground transmission systems," *IEEE Trans. Power Del.*, vol. 28, no. 4, pp. 2085–2092, Oct. 2013.
[16] L. Xu, P. Wang, L. Chen, and K. Wan, "Study on induced voltage compensation of 110kV power cable sheath," in *Proc. 4th Int. Conf. Electr. Eng. Control Technol. (CEECT)*, Shanghai, China, Dec. 2022, pp. 424–428.
[17] D. Ashlock, D. Perez-Liebana, and A. Saunders, "General video game playing escapes the no free lunch theorem," in *Proc. IEEE Conf. Comput. Intell. Games (CIG)*, Aug. 2017, pp. 17–24.
[18] J. Wu, W. Dai, Y. Wang, and B. Zhao, "Improved fruit fly optimization algorithm based on simulated annealing in neural network," in *Proc. Asia–Pacific Signal Inf. Process. Assoc. Annu. Summit Conf. (APSIPA ASC)*, Dec. 2021, pp. 100–105.
[19] R. K. Ranjan and V. Kumar, "A systematic review on fruit fly optimization algorithm and its applications," *Artif. Intell. Rev.*, vol. 56, no. 11, pp. 13015–13069, Mar. 2023.
[20] Y. Fan, P. Wang, M. Mafarja, M. Wang, X. Zhao, and H. Chen, "A bioinformatic variant fruit fly optimizer for tackling optimization problems," *Knowl.-Based Syst.*, vol. 213, Feb. 2021, Art. no. 106704.
[21] J. Cheng and T. Shi, "Structural optimization of transmission line tower based on improved fruit fly optimization algorithm," *Comput. Electr. Eng.*, vol. 103, Oct. 2022, Art. no. 108320.

SHYH-JIER HUANG (Senior Member, IEEE) received the Ph.D. degree in electrical engineering from the University of Washington, Seattle, WA, USA, in 1994. He is currently a Distinguished Professor with the Department of Electrical Engineering, National Cheng Kung University, Tainan, Taiwan. His current areas of research interests include power delivery, energy conversion, industrial electronics, and signal-processing applications. He received the Outstanding Research Award from the National Science Council of Taiwan, in 2004, the Outstanding Electrical Engineering Professor Award from the Chinese Institute of Electrical Engineering, in 2005, and the Outstanding Technical Achievement Award from the IEEE Tainan Section, in 2016. He served as the IEEE Taipei Chapter Chair for the IEEE Power Engineering Society, from 2002 to 2003.

CHAO-YUN TSAI received the B.S. degree in electrical engineering from the National Taipei University of Technology, Taipei, Taiwan, in 2021, and the M.S. degree in electrical engineering from National Cheng Kung University, Tainan, Taiwan, in 2023. His research interests include power system operation and artificial intelligence applications.

HSIANG-YU HSIEH received the B.S. degree in electrical engineering from the National Yunlin University of Science and Technology, Yunlin, Taiwan, in 2022. He is currently pursuing the M.S. degree with National Cheng Kung University, Tainan, Taiwan. His research interests include power system operation and artificial intelligence applications.

WEI-FU SU received the B.S. degree in electrical engineering from the National Taiwan University of Science and Technology, Taipei, Taiwan, in 1990, and the M.S. and Ph.D. degrees in electrical engineering from National Cheng Kung University, Tainan, Taiwan, in 1992 and 2001, respectively. Since 1992, he has been with the Department of Electrical Engineering, Kun Shan University, Tainan, Taiwan, where he is currently a Professor. His research interests include power quality, power system analysis, power electronics, and renewable energy.